Elsevier Editorial System(tm) for Nuclear Engineering and Design
Manuscript Draft

Manuscript Number: NED-D-11-00266R1

Title: Proposal of Failure Criterion Applicable to Finite Element Analysis Results for Wall-Thinned Pipes under Bending Load

Article Type: Full Length Article

Corresponding Author: Prof. Toshiyuki Meshii, Dr. Engng

Corresponding Author's Institution: University of Fukui

First Author: Toshiyuki Meshii, Dr. Engng

Order of Authors: Toshiyuki Meshii, Dr. Engng; Yoshiaki Ito, BS

Abstract: In this work, a failure criterion applicable to large strain Finite Element Analysis (FEA) results was proposed in order to predict both the fracture mode (collapse or cracking) and the limit bending load of wall-thinned straight pipes. This work was motivated from the recent experimental results of Tsuji and Meshii (2011); that is, fracture mode is not always collapse, and the fracture mode affects the limit bending load. The key finding in comparing their test results and a detailed large strain FEA results was that the Mises stress distribution at the limit bending load of a flawed cylinder was similar to that of a flawless cylinder; specifically, in case of collapse, the Mises stress exceeded the true yield stress of a material for the whole "volume" of a cylinder with a nominal wall thickness. Based on this finding, a failure criterion applicable to large strain FEA results of wall-thinned straight pipes under a bending load that can predict both fracture mode and limit bending load was proposed and was named the Domain Collapse Criterion (DCC). DCC predicts the limit bending load as the lower value of either the McFEA, which is the load at which the Mises stress exceeds the true yield strength of a straight pipe for the whole "volume" with a nominal wall thickness (fracture mode: collapse), or the McFEAb, which is the load at which the Mises stress in a section of the flaw ligament exceeds the true tensile stress (fracture mode: cracking). The results showed that the DCC could predict the fracture mode appropriately and the experimental limit bending load fundamentally on the conservative side within a maximum 20% difference regardless of the fracture mode. Another advantage of the DCC is that it uses the true yield and true tensile strength as the critical strength of the material and not the ambiguous flow strength.

***Highlights**

> A failure criterion applicable to large strain FEA results for wall-thinned straight pipes under a bending was proposed and named the Domain Collapse Criterion (DCC).

> The DCC predicted the limit bending load (LBL) conservatively and accurately, in an engineering sense.

> The fracture mode at LBL, i.e., whether cracking takes place or not, can be distinguished by the DCC.

> The DCC has an advantage on the point that it uses the true yield and the true tensile strength as the critical strength of the material and not the ambiguous flow strength.

*Title Page

Proposal of Failure Criterion Applicable to Finite Element Analysis Results for Wall-Thinned Pipes under Bending Load

Toshiyuki MESHII [a]*, Yoshiaki Ito [b]

[a] Professor, Graduate School of Engineering, University of Fukui, 3-9-1 Bunkyo, Fukui, Fukui, JAPAN.

[b] Graduate Student, University of Fukui, 3-9-1 Bunkyo, Fukui, Fukui, JAPAN.

*Correspondent, E-mail: meshii@u-fukui.ac.jp, FAX: +81-776-27-9764

Abstract

In this work, a failure criterion applicable to large strain Finite Element Analysis (FEA) results was proposed in order to predict both the fracture mode (collapse or cracking) and the limit bending load of wall-thinned straight pipes. This work was motivated from the recent experimental results of Tsuji and Meshii (2011); that is, fracture mode is not always collapse, and the fracture mode affects the limit bending load. The key finding in comparing their test results and a detailed large strain FEA results was that the Mises stress distribution at the limit bending load of a flawed cylinder was similar to that of a flawless cylinder; specifically, in case of collapse, the Mises stress exceeded the true yield stress of a material for the whole "volume" of a cylinder with a nominal wall thickness. Based on this finding, a failure criterion applicable to large strain FEA results of wall-thinned straight pipes

under a bending load that can predict both fracture mode and limit bending load was proposed and was named the Domain Collapse Criterion (DCC). DCC predicts the limit bending load as the lower value of either the M_c^{FEA}, which is the load at which the Mises stress exceeds the true yield strength of a straight pipe for the whole "volume" with a nominal wall thickness (fracture mode: collapse), or the M_c^{FEAb}, which is the load at which the Mises stress in a section of the flaw ligament exceeds the true tensile stress (fracture mode: cracking). The results showed that the DCC could predict the fracture mode appropriately and the experimental limit bending load fundamentally on the conservative side within a maximum 20% difference regardless of the fracture mode. Another advantage of the DCC is that it uses the true yield and true tensile strength as the critical strength of the material and not the ambiguous flow strength.

Key words: limit moment, bending, wall-thinned pipes, finite element analysis, fracture mode, cracking, collapse, and failure criterion.

Nomenclature

a: depth of a constant depth circumferential planar flaw (crack, Fig. 1)

p: internal pressure

t: wall thickness of a flawless cylinder

t_1, $t_{1Measured}$: flaw ligament thickness (design and measured value)

t_{min}: required minimum thickness

E: Young's modulus

L_e: considered length of the cylinder for the Domain Collapse Criterion application (Fig. 9)

L_n: length of the cylinder with a nominal wall thickness (Fig. 9)

M_c: limit bending load in general

M_c^{EXP}: limit bending load for this test system (obtained from the maximum applied load W_c as M_c^{EXP} = 0.1525 W_c kNm)

M, M_c^{FEA}, M_c^{FEAb}: moment, limit bending load predicted by the DCC for (corresponding to collapse and cracking) in this system, respectively. All of these moments are related to the applied load under consideration (W) as 0.1525 W kNm.

R: reaction force at the test specimen support (Fig. 4)

R_m, R_o: mean and outer radius of a flawless cylinder

W: applied load (Fig. 4)

X, Y, Z: coordinates for FEA (Fig. 4)

δ_z: axial length of a non-planar flaw

ε_{tp}: true plastic strain

ν: Poisson's ratio

θ: circumferential angle of a planar or a non-planar flaw

σ_n, σ_t: nominal and true stress

σ_{y0}, σ_y: nominal and true yield stress

σ_{B0}, σ_B: nominal and true tensile stress

1. Introduction

When evaluating the limit bending load of wall-thinned straight pipes, a limit moment equation for a circumferential crack inside a cylinder (Fig. 1, top), such as Kanninen's equation (Kanninen et al., 1978), is widely used (ANSI/ASME, 1991). This engineering judgment is not faulty because the limit moment of a crack (planar flaw) will probably give a conservative estimate for the flaws (non-planar flaw) in wall-thinned pipes. However, the following implicit limitations in applying the equation to non-planar flaws exist:

1) The fracture mode of a non-planar flaw under consideration is identical to that of the crack.

2) The effect of the axial length δ_z of the non-planar flaw (Fig. 1, middle and bottom), which is not considered for a circumferential crack on the limit moment M_c, is small or independent.

Concerning the fracture mode in 1), Miyazaki et al. (1999) pointed out that the fracture mode of wall-thinned pipes is not always collapse (ovalization) and that cracking can be observed for a specific combination of flaw configuration (Fig. 1, t_1 and θ). Note that their study was performed for a constant axial flaw length of the flaw δ_z and without internal pressure. However, an examination of the axial length of the wall thinning (Fig. 1, δ_z) is not necessarily sufficient.

The effect of δ_z on M_c in 2) has been examined by Han et al. (1999), Zheng et al. (2004) and Kim and Park (2006). They conducted limit-load analyses and obtained similar results: a) M_c monotonically decreased with the increase in δ_z and b) M_c converged to a lower bound for a flaw

with length of $\delta_z/(R_m\, t)^{0.5} > 1.5$ (R_m: mean radius of pipe, t: wall thickness). If these two findings are accepted, the M_c for a crack is larger than that for a non-planar flaw (wall thinning), and as a result, using the crack model for a non-planar flaw would be non-conservative. This curious finding might be a result of assuming that the fracture mode is always collapse.

Thus, in this work, attention was focused on the two implicit assumptions listed, and the effects that δ_z has on both the fracture mode and the limit bending load M_c were examined. From systematic tests of carbon pipes with artificial wall-thinned flaws under combined pressure and bending for constant flaw ligament of $t_1/t = 0.5$ (Tsuji and Meshii, 2011), it was found that i) cracking was observed for flaws with an aspect ratio of $\delta_z/(\theta R_m) < 0.25$ (circumstantially long flaws) and ii) M_c for a cracked cylinder was lower than that of a collapsed cylinder. Compared with the limit load analysis by Han et al. (1999), Zheng et al. (2004) and Kim and Park (2006), this experimental result is sufficient to show that the fracture mode (cracking or collapse) should be considered in evaluating the limit bending load of wall-thinned pipes. Finally, in this work, a large strain finite element analyses (FEA) were run to reproduce previous experiments (Tsuji and Meshii, 2011). By comparing the FEA results with the experimental results, a failure criterion applicable to the FEA result was proposed in order to predict both the fracture mode and the limit bending load of wall-thinned straight pipes. As a first step, flaws with a size of $\theta \leq \pi$ and subjected to tensile stresses were considered.

2. Experiments

The tested specimens were made of carbon steel JIS STPT370, with a nominal yield and a tensile stress of σ_{y0}=289 MPa and σ_{B0}=480 MPa, respectively. The nominal outer diameter and wall thickness of the tested pipes were 80 and t = 4 mm, respectively. The design value of the minimum wall thickness was set as t_{min} = 2 mm for all specimens to model the t_{min}/t = 0.5 pipes often found in nuclear power plants. The test specimen configuration and dimensions are shown in Fig. 2 and Table 1. The shaded part in column $t_{1Measured}$ in Table 1 shows that the ligament thickness for this groove-type flaw could not be measured.

All of the tests were conducted at room temperature. The pressure applied given by $p = p_{max}$ = 6.4 MPa was selected as the maximum rated pressure that corresponds to the t_{min} calculated based on JSME S NC1-2008 (JSME, 2008). The four-point bending test system is shown in Fig. 3. In the tests, the internal pressure p was first applied to a rated pressure of p_{max}, and the load W was applied gradually until a maximum load W_c was achieved. The maximum load W_c was defined as the two-second average around the observed maximum value and was measured at 0.01 second intervals. In this study, the bending load for this test system is $M = Wb/2 = 0.1525W$ kNm, and the limit bending load M_c^{Exp} in Table 1 is the M for the W_c obtained from the experiment. More details of the four-point bend test system are given in previous studies (Tsuji and Meshii, 2011).

3. Large strain FEA

Three-dimensional models of the pipes with flaws shown in Table 1 and Fig. 2, and without flaws were developed using the MARC finite element code with models containing mesh refinement at the wall-thinned zone. In each case, one quarter of the specimen was modeled, as shown in Fig. 4, by applying symmetry conditions. All models used 8-noded brick elements. Note that the flaw was inserted in the lower portion of the cylinder in agreement with Fig. 2 such that a tension bending stress was applied.

For all analyses, the material behavior was assumed to be governed by the J2-incremental theory of plasticity, the isotropic hardening rule and the Prandtl-Ruess flow rule. The Young's modulus E was equal to 206 GPa, and the Poisson's ratio ν was 0.3. The true stress σ_t -true strain (plastic) ε_{tp} curve used in the large strain FEA is shown in Fig. 5. σ_t and ε_{tp} were evaluated under the constant volume assumption such that $\sigma_t = \sigma_n (1+\varepsilon_n)$ and $\varepsilon_{tp} = \ln (1+\varepsilon_n) - \sigma_t/E$, where σ_n is the nominal stress and ε_n the nominal strain obtained from a tensile test. The tensile test used a JIS sub-size test specimen of 3 mm in diameter cut out from the pipe in the axial direction. The true yield and tensile strengths were σ_y = 291 MPa and σ_B = 591 MPa, respectively. Though the constant volume assumption is not valid over σ_B, the σ_t - ε_{tp} curve was expanded over σ_B in order to make a numerical analysis up to the load corresponding to the local equivalent stress of σ_B. However, as shown later, all the FEA results were evaluated below a local equivalent stress of σ_B, and therefore

did not violate the constant volume assumption.

The boundary conditions are shown in Fig. 4. In addition to the applied load (W/4), the internal pressure p = 6.4 MPa and uniform thrust stress σ_z = 8.27 MPa on the cylinder end, which corresponded to p, were applied as initial loads. The maximum applied load (W_{max}/4) was selected as 25 kN, considering that the actuator capacity of the testing apparatus was 100 kN. (W/4) in the range of 0 up to the load at which the outer surface axial stress of the flawless cylinder reached the $0.2\sigma_{y0}$ was applied in three even incremental loading steps. After this loading, MARC's automatic load stepping option was applied up to the maximum load under the restriction that the strain increment in a given load increment was less than 2% of the previous total strain. In addition, MARC's "follower force" option was specified in order to ensure that the geometric non-linear effects were included, and therefore the internal pressure was always applied perpendicular to the current (deformed) inner surface of the cylinder. To avoid local large deformation at the loaded node and at the supported node as seen in Fig. 4, the material of the elements surrounding these nodes were set as linearly elastic as shown in Fig. 6.

4. Proposal of Failure Criterion Applicable to FEA Results for Wall-Thinned Pipes under Bending Load

4.1 Point of view

The deformation of the straight pipes at the limit bending load was identical with or without flaws due to wall thinning. For flawless straight pipes, the mechanism of collapse has been an issue of interest since the 1920s, and there seems to be a common agreement on the mechanism, as follows:

1) local buckling due to maximum compression stress due to bending deformation (Seide and Weingarten, 1961)

2) ovalization of the circular cross-section of the pipe due to a bending load (Brazier, 1927).

These phenomena are similar for wall-thinned straight pipes (Miyazaki et al., 1999) and 2) for the pipes summarized in Table 1. Thus, if the findings of Miyazaki et al. are accepted, the gross stress distribution in straight pipes with and without flaws might be similar.

If the above point of view is accepted, the famous collapse criterion for a perfectly elastic-plastic beam, shown in Fig. 7, can be considered as stress exceeding the critical material strength for the whole "volume" of a pipe.

The gross deformation for flawless and flawed straight pipes are similar at the limit bending load, but because the stress at a specific cross-section for flawless and flawed pipes is not the same, the Mises stress distribution in a specific volume during the load increment was studied. For this purpose, a large strain FEA for flawless pipes with a wall thickness of t = 4 mm was also conducted as a reference.

4.2 Mises stress distribution change under load increment

4.2.1 Mises stress distribution change under load increment for a flawless cylinder

The Mises stress distribution change under a load increment in the flawless cylinder is summarized in Fig. 8. In this figure, the yielded zones that corresponds to Mises stress exceeding the true yield stress σ_B = 291 MPa is colored red. M_c^{FEA}, which appears in these figures, is the bending load corresponding to the load step when all of the volume of the nominal wall thickness t=4 mm, shown in Fig. 9 left (in concrete, $|Z| \leq L_n/2$ = 120 mm), yielded. For this decision, the Mises stress obtained at the integration point was extrapolated to the nodes using the element shape function and averaged when a node was shared by multiple elements. Because the stress extrapolated to the nodes in the section near the thickness change tends to be inaccurate, two layers adjacent to this section were excluded as shown in Fig. 9 on the right (in concrete, the volume for evaluation was set as $|Z| \leq L_e/2$). Note that the bending load shown in Fig. 8 was calculated from the applied load (W/4) as $M = Wb/2 = 0.1525W$ kNm, which was identical to that used in the experiment.

Fig. 8 shows that the Mises stress gradient in the axial direction could not be observed for the volume in which t=4 mm ($|Z| \leq L_e/2$) for all loads, which is naturally expected from beam theory. On the other hand, the stiffened portion ($L_n/2 \leq |Z| \leq 175$ mm) did not yield for loads under M_c^{FEA}. The "section" yielding (Z = 0) was automatically equal to the yielding of the "volume" with t=4 mm. Though no experimental result corresponding to this case exists, this M_c^{FEA} was assumed to be a

candidate for the limit bending load.

4.2.2 Validation of the FEA results for flawed cylinders

Before proceeding to examine the Mises stress distribution change under the load increment for flawed cylinder, the FEA results were compared to the experimental results in order to validate the FEA. Here, typical examples of collapse ($\delta_z/(\theta R_m)$ = 1.005) and cracking ($\delta_z/(\theta R_m)$=0.168) were considered. The FEA results were plotted up to the bending load M_c^{FEA}, which is the possible limit bending load determined by the procedure previously mentioned for the flawless cylinder. All of the experimental data was acquired every 0.01 second and displayed in the figures at every second for load vs. load-line displacement and every 0.1 second for load vs. strain.

From the load vs. load-line displacement shown in Fig. 10, it is seen that both the bending load and displacement at the limit bending load for the case of collapse (Fig. 10 left) were larger than those for the case of cracking (Fig. 10 right), as expected. It is also seen that the FEA result predicted the limit bending load closely and on the conservative side. The limit bending load for 7 out of a total of 8 collapsed-specimen cases and 6 out of 7 cracked-specimen cases were predicted on the conservative side by M_c^{FEA}, as shown in Table 1. On the other hand, a discrepancy can be seen for the predicted and measured displacement at the limit bending load. The FEA results overestimated this displacement in the case of collapse (Fig. 10 left), and underestimated the value in the case of cracking (Fig. 10 right). However, the FEA load vs. load-line displacement path was close to the

experimental results for all the tested specimens; these results are shown in Table 1.

The location of strain measurement by two strain gauges was on the symmetry plane (Z = 0), as shown in Fig. 4. Strain gauge 1 was located on the tension side (X = 0, Y = −40 mm in Fig. 4) and strain gauge 2 was located on the compression side (X = 0, Y = 40 mm in Fig. 4). Both gauges had a nominal measurement range of 20%. Here again, typical examples for collapse: $\delta_z/(\theta R_m) = 1.005$ and cracking: $\delta_z/(\theta R_m) = 0.168$ were considered and are summarized in Figs. 11 and 12, respectively. It was seen from all the experimental results, Figs. 11 and 12 that a strain increment without a load increment was observed at the initiation of yielding. This finding seems to correspond to the fact that the specimen material STPT370 showed a lower and an upper yield point. On the other hand, the FEA model excluded the upper yield point, but the overall load vs. strain relationship showed good agreement, considering the fact that the reading in strain gauge 2 for both the collapse and the cracking became distorted near the limit load. A similar tendency was also observed for the other cases.

By examining Figs. 10 through 12 and in the other cases, it was concluded that the FEA results demonstrated a good agreement with the experimental results overall.

4.2.3 The Mises stress distribution change under a load increment for flawed cylinders

Next, the Mises stress distribution change under a load increment was examined. Figs. 13 and 14 show typical results for the cases with flaws that experienced collapse ($\delta_z/(\theta R_m)$=1.005) and cracking

($\delta_z/(\theta R_m)$=0.168), respectively, at the limit bending load. Again in these figures, the yield zones that corresponds to the Mises stress that exceed the true yield stress σ_y = 291 MPa are colored red. M_c^{FEA}, which appears in these figures, is the bending load corresponding to the load step in which all of the volume of the nominal wall thickness t=4 mm, shown in Fig. 9 right, yielded. In Fig. 13, the wall-thinned portion under a tension bending load first started to yield from the outer surface as expected. At a load of M/ M_c^{FEA} = 0.48, the ligament of this flaw yielded throughout the outer to inner surface of the cylinder, but in comparison with the experimental limit bending load M_c^{Exp} presented in Table 1, it is clear that the failure was not observed at this load. When the load increased to M/M_c^{FEA} = 0.75, the symmetry plane of Z = 0 together with the region containing flaw (in concrete, $|Z| \leq \delta_z/2$) was approximately yielded, even though the load was sufficiently below M_c^{Exp}. The safety margin in the "section" yield failure criterion (such as Net Section Collapse Criterion by Kanninen et al., 1978) seemed to be the remaining elastic volume for a pipe cross section with t=4 mm. After the region containing the flaw ($|Z| \leq \delta_z/2$) yielded, as seen in a case of M/M_c^{FEA} = 0.83, the expansion of the yielded region outside $|Z| \leq \delta_z/2$ (i.e., $\delta_z/2 < |Z| \leq L_e$) was similar to the case of flawless cylinder. Finally, for a load of M/ M_c^{FEA} = 1, all of the volume for a cross-section of t=4 mm yielded. As shown in Table 1, M_c^{EXP}/M_c^{FEA} = 1.01 and M_c^{FEA} predicted the experimental result accurately and on the conservative side for this case. As seen in Table 1 and Fig. 16, M_c^{FEA} predicted the limit bending load on the conservative side for 7 out of 8 cases in which the fracture mode was

collapse and was in the range of M_c^{EXP}/M_c^{FEA} = 1.01~1.14. The only non-conservative case was test specimen no. 10-18, in which M_c^{EXP}/M_c^{FEA} = 0.97. Overall, it was concluded that in case the fracture mode was collapse, M_c^{FEA} predicted the limit bending load accurately in an engineering sense.

Fig. 14 is a typical Mises stress distribution change under load increment for cases with flaws that experienced cracking at the limit bending load. The flaw aspect ratio was $\delta_z/(\theta R_m)$ = 0.168 for this case. The definitions of M_c^{FEA} and the color scale are identical within the scales in Figs. 8 and 13. It can be seen in Fig. 14 that the characteristic of the Mises stress distribution resembled that of Fig. 13, even though the fracture mode was cracking.

For example, in the case of M/M_c^{FEA} = 0.61, it is seen that the Mises stress in the flawed ligament has completely exceeded σ_y. After the region containing the flaw ($|Z| \leq \delta_z/2$) yielded at M/M_c^{FEA} = 0.88, the expansion of the yielded region outside of $|Z| \leq \delta_z/2$ (i.e., $\delta_z/2 < |Z| \leq L_e$) was similar to the case of flawless cylinder.

The difference in the Mises stress distribution was found when the color scales in Fig. 14 were redefined such that the gray color represented the Mises stress exceeding true tensile stress σ_B = 591 MPa as shown in Fig. 15. In this figure, the flawed ligament is highlighted. The definition of M_c^{FEA} in this figure is identical to the definition used in Figs. 8, 13 and 14. It is seen from Fig. 15 that the Mises stress started to exceed σ_B from the inner surface at M/M_c^{FEA} = 0.977, and the region exceeding σ_B subsequently penetrated the flaw ligament at M/M_c^{FEA} = 0.979. This observation

seemed to correspond to the experimental fact that cracks penetrated from the inner surface to outside for this test specimen. Thus, the bending load at which the Mises stress exceeded σ_B throughout the flaw ligament was designated as M_c^{FEAb} and is summarized in Table 1 and Fig. 16, including other cases. As seen in Table 1, M_c^{FEAb} was smaller than M_c^{FEA} for all of the cases that experienced cracking. Conversely, M_c^{FEAb} was larger than M_c^{FEA} for all of the cases the fracture mode was collapse. These results seemed to indicate that the fracture mode can be predicted by comparing M_c^{FEAb} and M_c^{FEA}.

Also seen in Table 1, M_c^{FEAb} predicted the limit bending load on the conservative side for 6 out of 7 cases in which the fracture mode was cracking and M_c^{EXP}/M_c^{FEAb} ranged from 1.05 to 1.18. The only non-conservative case was test specimen no. 10-15 in which $M_c^{EXP}/M_c^{FEAb} = 0.94$. Though the discrepancy in prediction of the limit bending load in the case of cracking was larger than that of collapse, the discrepancy was less than 20%. Considering the fact that axial flaw length δ_z was small as 1 mm and very sensitive to the manufactured ligament thickness for the non-conservative case, it is concluded that M_c^{FEAb} predicted the limit bending load accurately in an engineering sense.

Although not shown in Table 1, M_c^{FEAb} was close to M_c^{FEA} for the case of cracking, as shown in Fig. 15. Because the failure criterion corresponding directly to the fracture mode seemed to be preferable, the lower value of M_c^{FEAb} and M_c^{FEA} was listed in Table 1.

4.3 Proposal of failure criterion applicable to FEA results for wall-thinned pipes under bending load

According to the discussions above, the limit bending load M_c^{FEA}, which corresponds to a fracture mode of collapse, is a state in which the Mises stress exceeds the true yield strength of the material in the "volume" of a straight pipe with a nominal wall thickness regardless of the presence of a flaw. If there is an elastic portion remaining in this volume, the pipe, as a gross structure, still has the capability to carry more loads and will not collapse. The deformation of a straight pipe was similar with or without flaws (Miyazaki et al., 1999). If the limit bending load M_c^{FEAb}, which is the load in which the Mises stress exceeds the true tensile stress throughout the flaw ligament, is smaller than M_c^{FEA}, then cracking occurs.

Thus, in summary, a failure criterion applicable to the large strain FEA results for wall-thinned pipes under bending was proposed using the following three-step procedures and was named the Domain Collapse Criterion (DCC).

(1) Evaluate the bending load at which the Mises stress exceeds the true yield strength of the material for the whole "volume" of a straight pipe with a nominal wall thickness (M_c^{FEA}).

(2) Check whether the Mises stress at a flaw ligament exceeds the true tensile stress below M_c^{FEA}. In this case, the limit bending load is adjusted to this lower value M_c^{FEAb}.

(3) Predict the fracture mode, in the case that the limit bending load is M_c^{FEAb}, failure is through cracking, and any other case indicates collapse.

5. Discussion

A failure criterion to predict the limit bending load of wall-thinned straight pipes, which is applicable to large strain FEA results was proposed and named the DCC. The DCC predicts the limit bending load as the lower value of M_c^{FEA}, which is the load at which the Mises stress exceeds the true yield strength of a material for the whole "volume" of a straight pipe with a nominal wall thickness, or M_c^{FEAb}, which is the load at which the Mises stress in a section of the flaw ligament exceeds the true tensile stress.

There might be a concern that the proposed DCC for collapse does not consider the real local effects due to the artificial flaw. However, as mentioned for the case in Fig. 13, local effects were naturally considered, as seen in the example that experienced a load of M_c^{EXP}/M_c^{FEAb} = 0.55 or 0.88, but the local section yielding in the flaw ligament or in the cross section Z = 0 did not cause collapse. Collapse occurred under the load, when the whole "volume" of a straight pipe with a nominal wall thickness yielded. This result supports our point of view that the gross deformations for the flawless and flawed pipes are similar at the limit bending load for the case of collapse.

A strong point of the DCC is that it can appropriately and seamlessly handle the fracture mode of a wall-thinned pipe at the limit bending load. The results in Table 1 indicate that the DCC overcame the curious results obtained by running a limit load analysis and evaluating the limit load under the assumption that the fracture mode is always collapse (Han et al., 1999). In concrete, M_c

monotonically decreases with an increase in δ_z, and M_c converges to a lower bound for a flaw with length of $\delta_z/(R_m t)^{0.5} > 1.5$ (R_m: mean radius of pipe, t: wall thickness).

Another advantage of the DCC is that it uses the true yield and the true tensile strength as the critical strength of the material, and not the flow strength. Because the definition of the flow strength is ambiguous (i.e., the average of the yield and tensile strength (ASME, 2004; JSME, 2004), yield strength + 10 ksi (Kiefner et al., 1973), yield strength divided by 0.9 (API, 2000) and 1.1 times the yield strength (ANSI/ASME, 1991) or tensile strength (Leis and Stephens, 1997)), the clear physical meaning of the critical strength in DCC has an advantage.

The DCC predicted the limit bending load on the conservative side for 13 out of a total of 15 tests. The discrepancy for the two non-conservative predictions was 3 and 6%, as shown in Table 1. The maximum discrepancy on the conservative side was 18%. The DCC generally was accurate in the case of collapse, but the accuracy decreased for a narrow grooved-type flaw. These results are acceptable, in the sense that the DCC can seamlessly predict the limit bending load regardless of the fracture mode (that is, the discrepancy change due to change in fracture mode was negligible).

However, at this time, more work should be done to "digitally" define the limit bending load, or in concrete, work should be done to define at what load the Mises stress on the neutral plane of bending exceeds the yield strength. Our mesh generation introduced in this work located nodes very close to the neutral axis, and the stresses derived on the integration point were linearly extrapolated

to the nodes and averaged for the elements that shared the node. The stress evaluation at the nodes in this style is the main cause of the error of the limit bending load, and future work includes improvements in this error.

6. Conclusion

In this paper, the problem of axial length δ_z of a non-planar flaw in a wall-thinned pipe affecting both the fracture mode (collapse or cracking) and the limit bending load, which was recently pointed out by Tsuji and Meshii (2011) from their test results, was considered. By comparing their test results with a detailed large strain FEA results, it was found that the bending load at which the flaw ligament or the net section of a flaw yielded had enough margin to the limit bending load regardless of the fracture mode. The Mises stress distribution at the limit bending load for the flawed cylinder indicated that this distribution was similar to that for a flawless cylinder, at the point that the Mises stress exceeded the true yield stress of a material for the whole "volume" of a straight pipe with a nominal wall thickness in the case of collapse. Conversely in case of cracking, the ligament Mises stress exceeded the true tensile stress before reaching the previously mentioned collapse condition.

Because the fracture mode correlated with the limit bending load and the existing failure criterion usually assumed that the fracture mode was collapse, a failure criterion that is applicable to large strain FEA results for a wall-thinned straight pipes under a bending load that can predict both

fracture mode and limit bending load was proposed from the results obtained. The criterion was named the Domain Collapse Criterion (DCC). The DCC predicts the limit bending load as the lower value of either M_c^{FEA}, which is the load at which the Mises stress exceeds the true yield strength of a material for the whole "volume" of a straight pipe with a nominal wall thickness (fracture mode: collapse), or M_c^{FEAb}, which is the load at which the Mises stress in a section of the flaw ligament exceeds the true tensile stress (fracture mode: cracking).

Results demonstrated that the DCC could predict the fracture mode for all the test specimens considered. The DCC predicted the limit bending load on the conservative side for 15 out of a total of 17 specimens, and the maximum discrepancy was 18%. The maximum discrepancy for the non-conservative estimate was 6%. Thus, it is concluded that it is now possible to predict the effect of the axial length δ_z of a non-planar flaw in a wall-thinned pipe on the fracture mode (collapse or cracking) and the limit bending load by running a large strain FEA and by applying the DCC to the results.

Another advantage of the DCC is that it uses the true yield and the true tensile strength as the critical strength of the material and not the flow strength. Because the definition of the flow strength is ambiguous, the clear physical meaning of the critical strength in the DCC has an advantage.

Acknowledgement

This project was done under the supports of the NISA project on Enhancement of Ageing Management and Maintenance of Nuclear Power Stations. Their support is greatly appreciated. The author also thanks the students and staffs who participated in this project.

List of Tables

List of Figures

Spec.10-12)

Fig. 15 The Mises stress distribution at M_c^{FEA} (case of cracking: $\delta_z/(\theta R_m)$=0.168 Spec.10-04; 591 MPa is true tensile stress)

Fig. 16 Comparison of the limit bending load using the DCC: M_c^{FEA}, M_c^{FEAb} and by experiment: M_c^{EXP}

*Bibliography
Click here to view linked References

References

API, 2000. Fitness-For-Service API579. American Petroleum Institute, Washington, D.C.

ANSI/ASME, 1991. Manual for determining the remaining strength of corroded pipeline, B31.G. The American Society of Mechanical Engineers, New York.

ASME, 2004. Boiler and Pressure Vessel Code Section XI, The American Society of Mechanical Engineers, New York.

Brazier, L., 1927. On the flexure of thin cylindrical shells and other" thin" sections. Proceedings of the Royal Society of London. Series A 116, 104-114.

Han, L.-H., He, S.-Y., Wang, Y.-P., Liu, C.-D., 1999. Limit moment of local wall thinning in pipe under bending. International Journal of Pressure Vessels and Piping 76, 539-542.

JSME, 2004. Codes for Nuclear Power Generation Facilities: Rules of Fitness for-Service for Nuclear Power Plants, The Japan Society of Mechanical Engineers, Tokyo.

JSME, 2008. S NC1-2008: Code for nuclear power generation facilities - rules on design and construction for nuclear power plants. The Japan Society of Mechanical Engineers, Tokyo.

Kanninen, M.F., Broek, D., Hahn, G.T., Marschall, C.W., Rybicki, E.F., Wilkowski, G.M., 1978. Towards an elastic-plastic fracture mechanics predictive capability for reactor piping. Nuclear Engineering and Design 48, 117-134.

Kiefner, J.F., Maxey, W.A., Eiber, R.J., Duffy, A.R., 1973. Failure stress levels of flaws in pressurized cylinders. ASTM STP 536, 461–481.

Kim, J.W., Park, C.Y., 2006. Experimental investigation of the failure behavior of notched wall-thinned pipes. Nuclear Engineering and Design 236, 1838-1846.

Leis, B.N., Stephens, D.R., 1997. An alternative approach to assess the integrityof corroded line pipe—Part II: alternative criterion. In: 7th Int. Offshore and Polar Engineering Conference, vol. IV, pp. 635–641.

Miyazaki, K., Kanno, S., Ishiwata, M., Hasegawa, K., Hwan Ahn, S., Ando, K., 1999. Fracture behavior of carbon steel pipe with local wall thinning subjected to bending load. Nuclear Engineering and Design 191, 195-204.

Seide, P., Weingarten, V., 1961. On the buckling of cylindrical circular shells under pure bending. Journal of Applied Mechanics 28, 112-116.

Tsuji, M., Meshii, T., 2011. Proposal of limit moment equation applicable to planar/non-planar flaw in wall thinned pipes under bending. Nuclear Engineering and Design 241, 4089-4094. doi:10.1016/j.nucengdes.2011.08.037.

Zheng, M., Luo, J.H., Zhao, X.W., Zhou, G., Li, H.L., 2004. Modified expression for estimating the limit bending moment of local corroded pipeline. International Journal of Pressure Vessels and Piping 81, 725-729.

Table

Table 1 Dimensions of the artificial flaws, limit bending load and fracture mode of the specimen

$\theta/2\pi$	δ_z mm	$t_{1\text{Measured}}$ mm	$\frac{\delta_z}{\theta R_m}$	M_c^{Exp} kNm	M_c^{FEA} kNm	M_c^{FEAb} kNm	$\frac{M_c^{Exp}}{M_c^{FEA}}$	$\frac{M_c^{Exp}}{M_c^{FEAb}}$	Fracture Mode	Predicted Fracture Mode	Ser. # (flaw type in Fig. 2)
1/2	140	2.08	1.173	6.85	6.68	>6.68	1.02		Collapse	Collapse	10-03 (a)
	20	1.96	0.168	7.51	>7.03	7.03		1.07	Crack	Crack	10-04 (a)
1/3	107	2.08	1.344	7.52	7.26	>7.26	1.04		Collapse	Collapse	10-05 (a)
	20	1.95	0.251	8.31	>7.37	7.37		1.13	Crack	Crack	10-07 (a)
	10	2.04	0.126	8.46	>7.18	7.18		1.18	Crack	Crack	10-08 (a)
	1	1.96	0.013	6.68	>7.10	7.10		0.94	Crack	Crack	10-15 (c)
1/6	74	2.09	1.86	8.62	8.05	>8.05	1.07		Collapse	Collapse	10-11 (a)
	40	2.04	1.005	8.75	8.68	>8.68	1.01		Collapse	Collapse	10-12 (a)
	10	2.00	0.251	8.81	>8.00	8.00		1.10	Crack	Crack	10-13 (a)
	6	1.97	0.151	8.70	>7.71	7.71		1.13	Crack	Crack	10-14 (a)
	1	2.05	0.025	8.10	>7.69	7.69		1.05	Crack	Crack	10-16 (c)
1/20	12	2.11	1.005	9.73	8.53	>8.53	1.14		Collapse	Collapse	10-10 (a)
	6	2.08	0.503	9.40	8.34	>8.34	1.13		Collapse	Collapse	10-19 (b)
1/200	20	2.03	16.75	9.56	9.54	>9.54	1.00		Collapse	Collapse	10-17 (b)
	10	2.04	8.377	9.24	9.54	>9.54	0.97		Collapse	Collapse	10-18 (b)

Figure

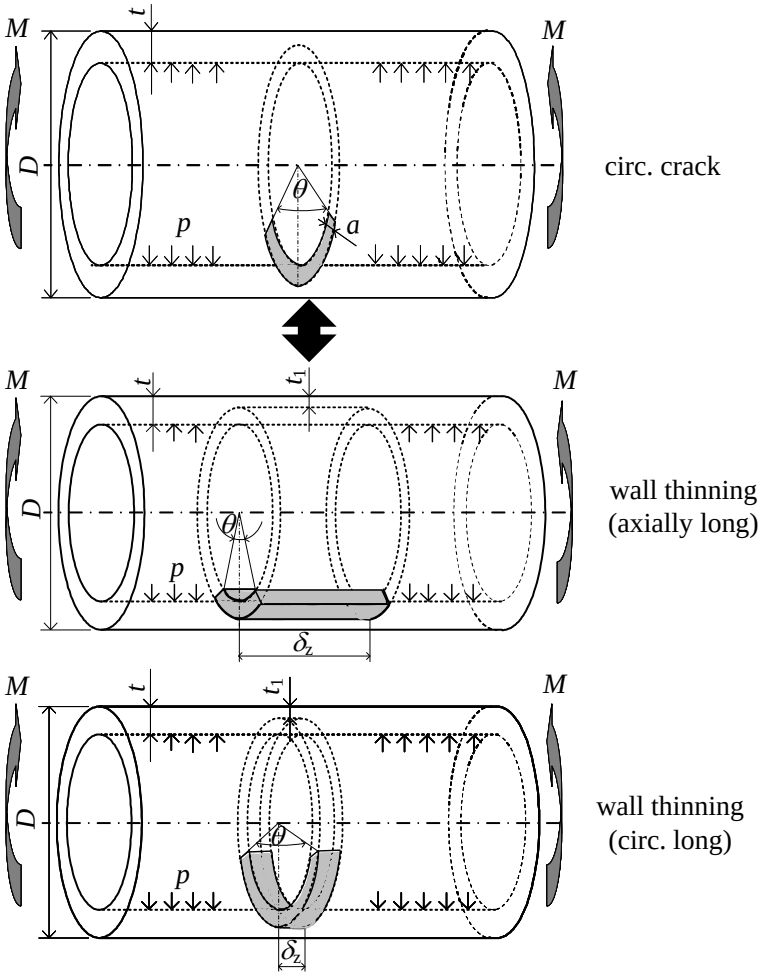

	crack	wall thinning
flaw depth	a	t-t_1
axial length		δ_z
circ. length	θ	θ

Fig. 1 Circumferential planar flaw and non-planar flaws (axially and circumferentially long) in a cylinder

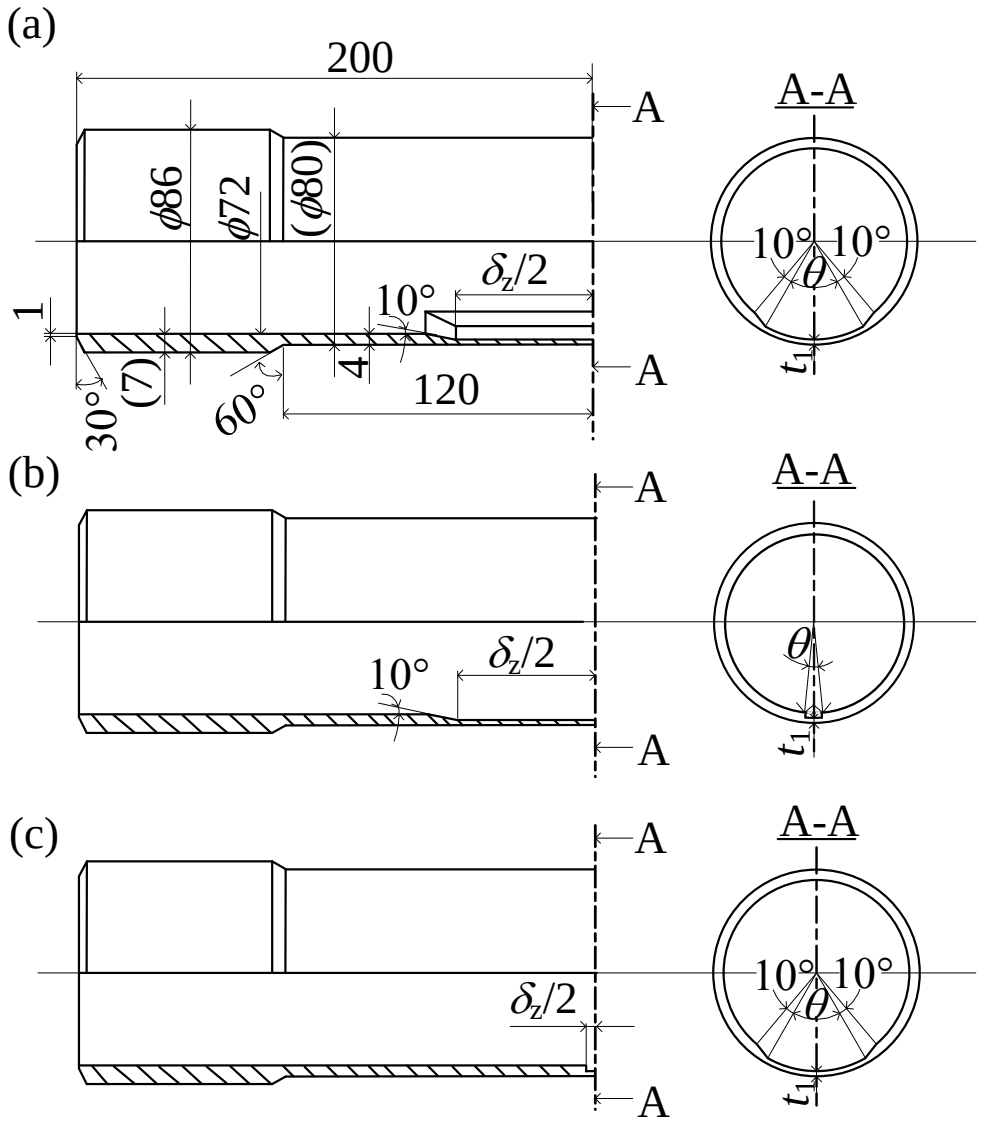

Fig. 2 Test specimen configuration

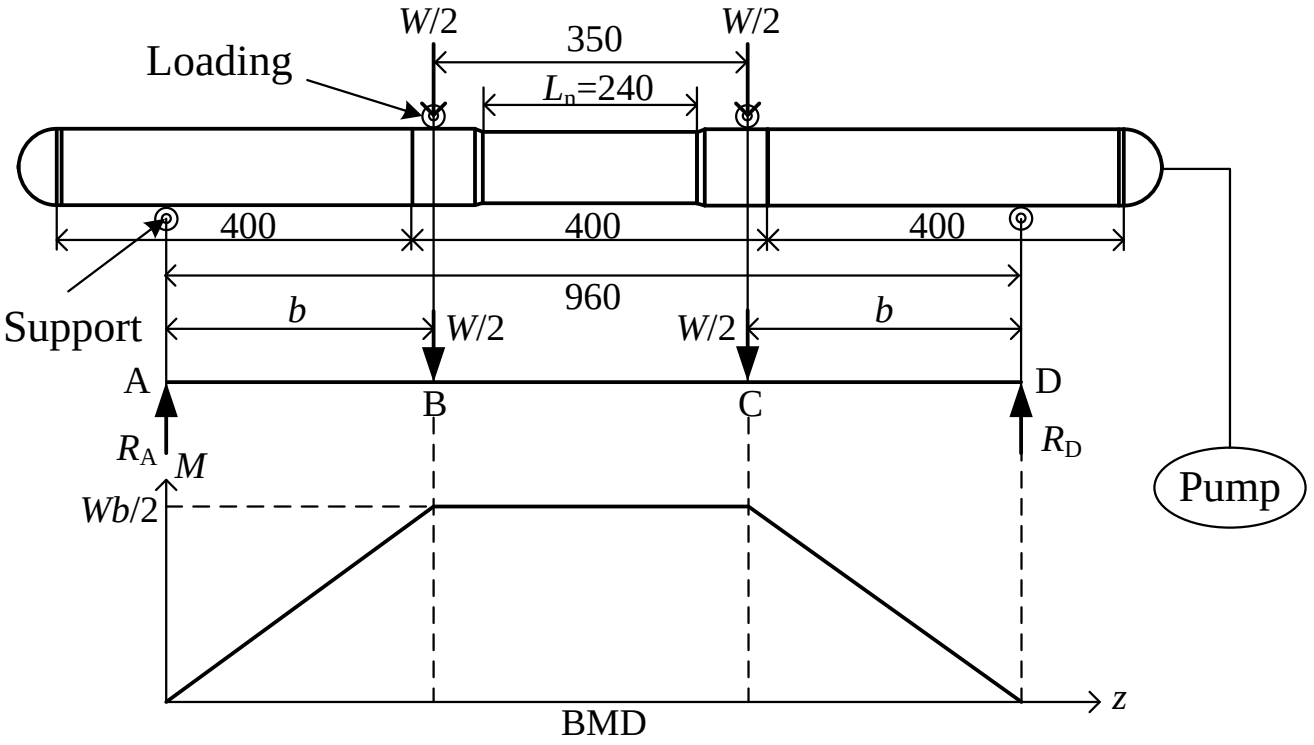

Fig. 3 The four-point bending test and bending moment diagram (unit: mm)

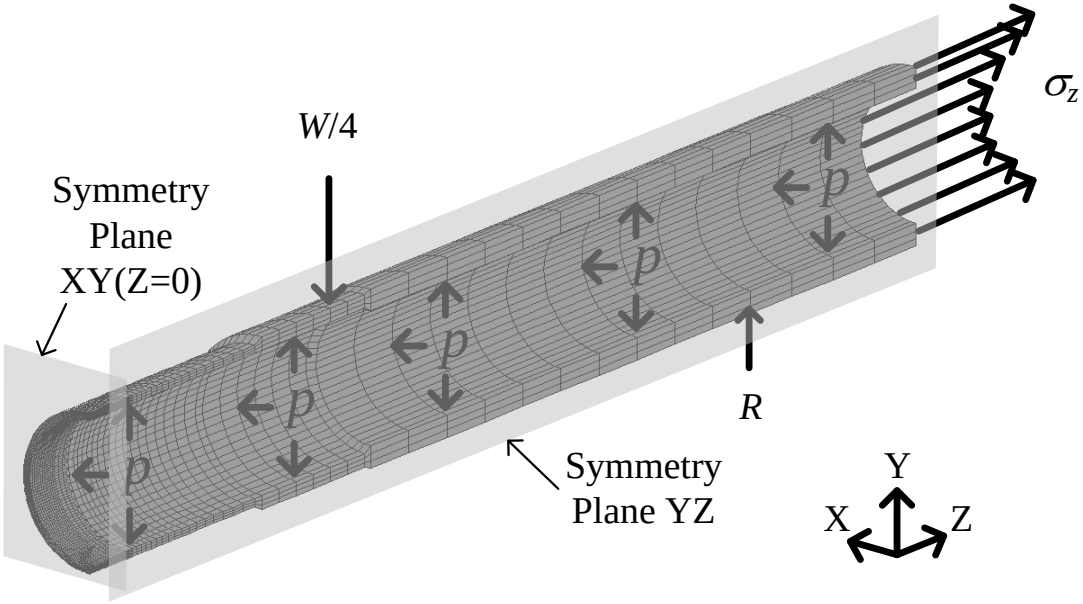

Fig. 4 The FEA model and boundary conditions

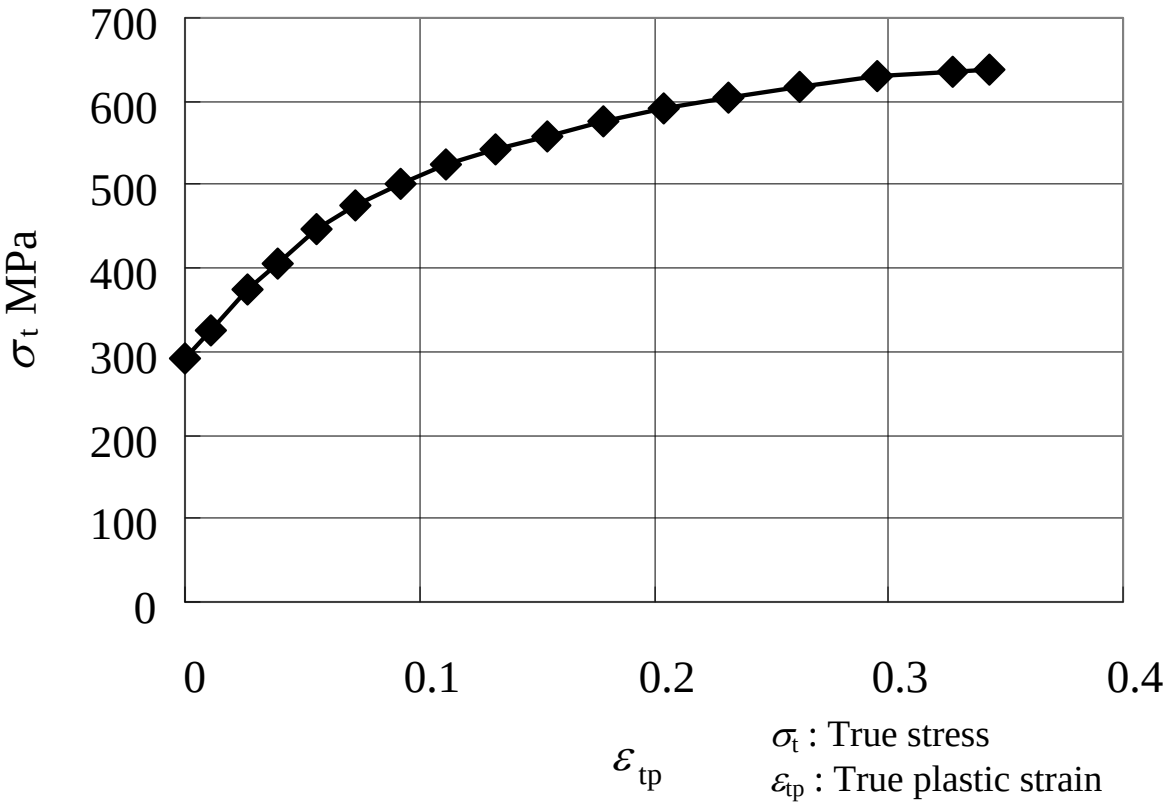

Fig. 5 The true stress-true strain (plastic) diagram

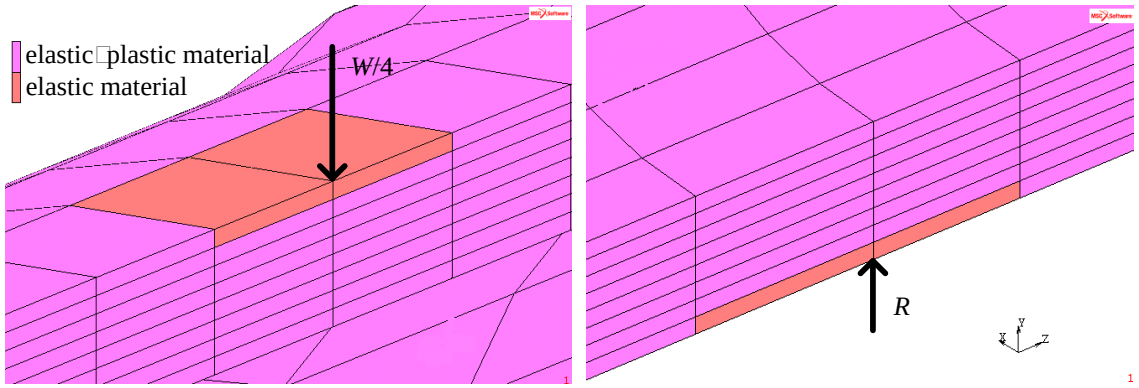

Fig. 6 Special treatment for elements around the loaded and supported nodes

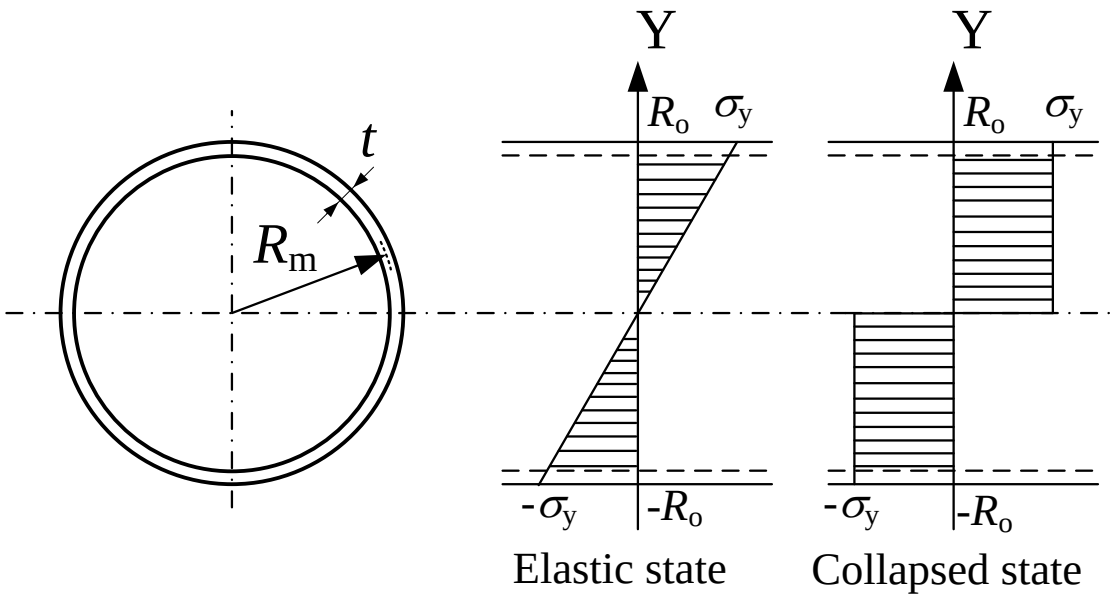

Fig. 7 Collapse of a thin pipe under a bending load

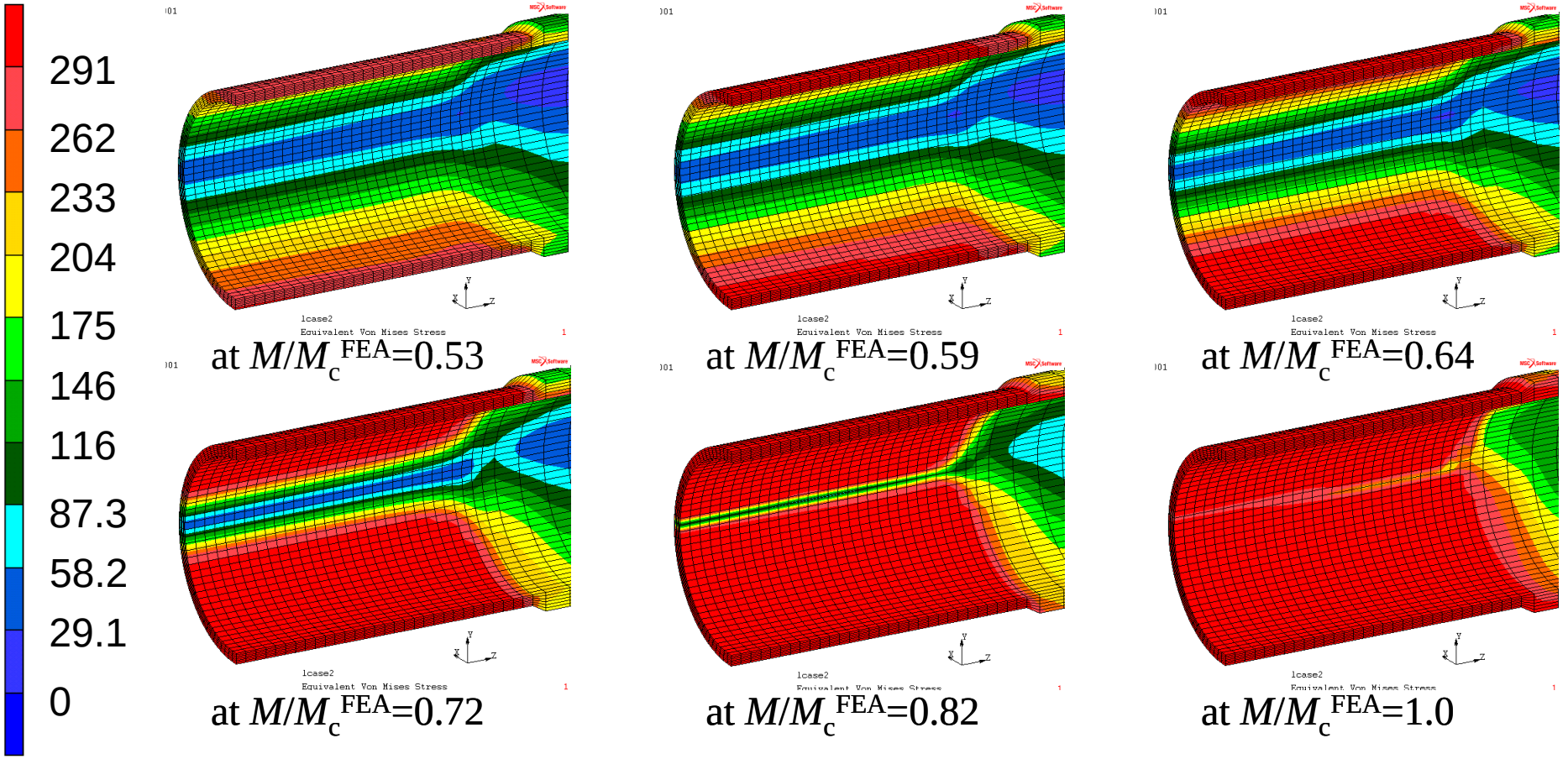

Fig. 8 The Mises stress distribution change for an increasing load (case without flaw)

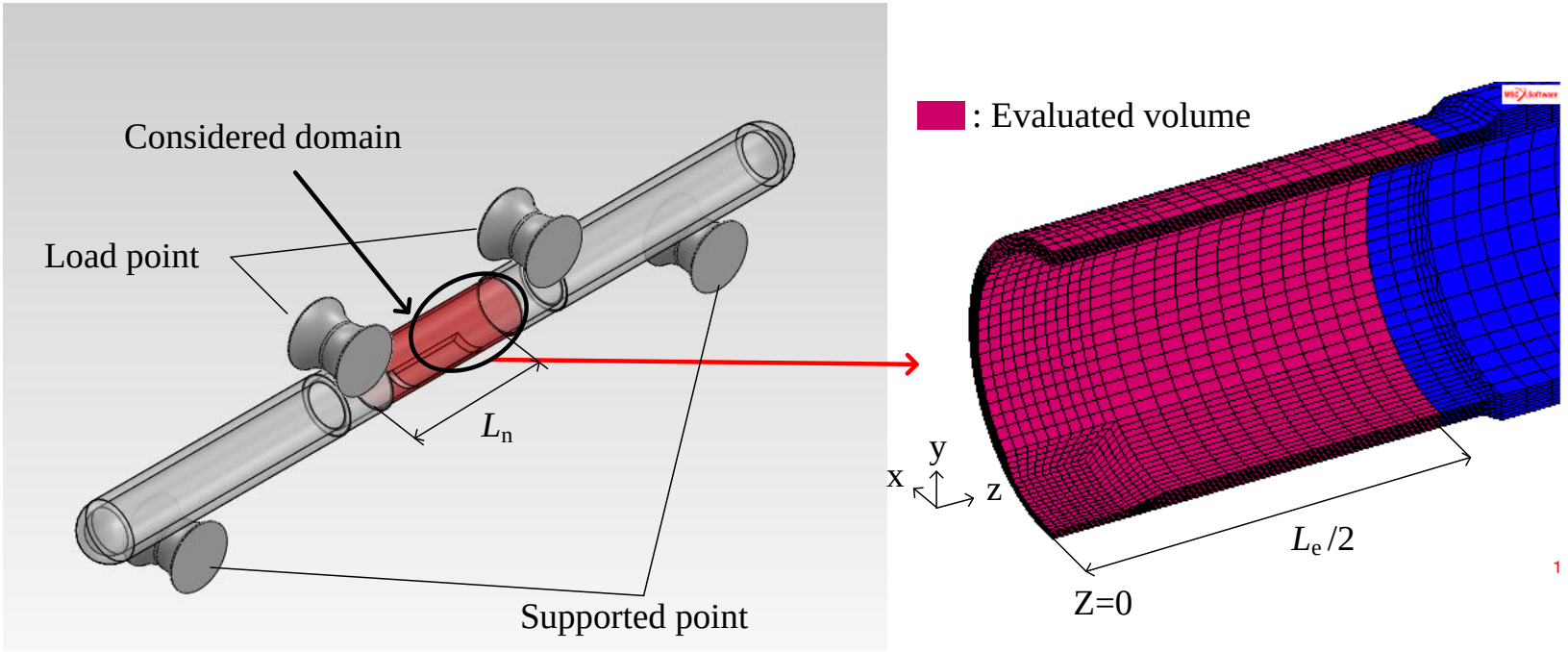

Fig. 9 The considered and evaluated domain

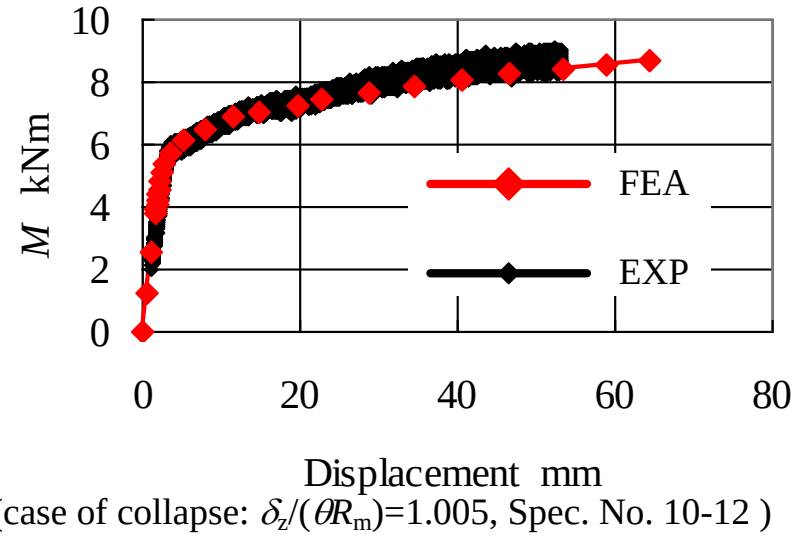

(case of collapse: $\delta_z/(\theta R_m)$=1.005, Spec. No. 10-12)

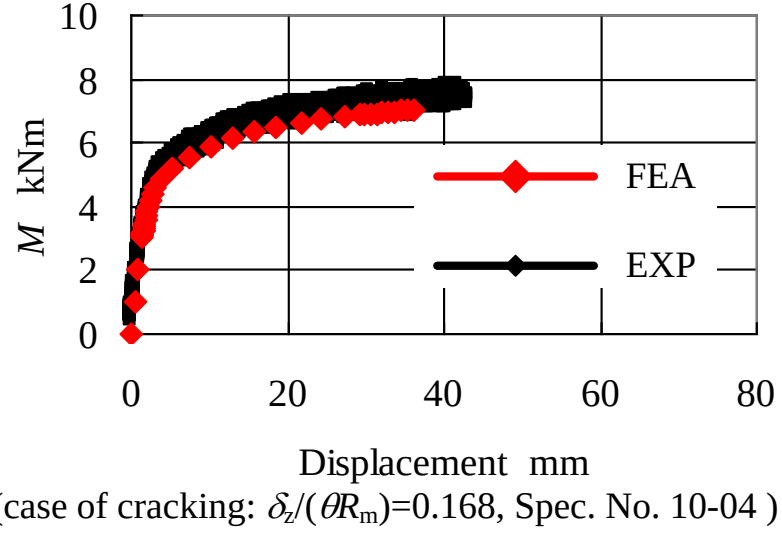

(case of cracking: $\delta_z/(\theta R_m)$=0.168, Spec. No. 10-04)

Fig. 10 Comparison of the FEA and experimental results: load vs displacement

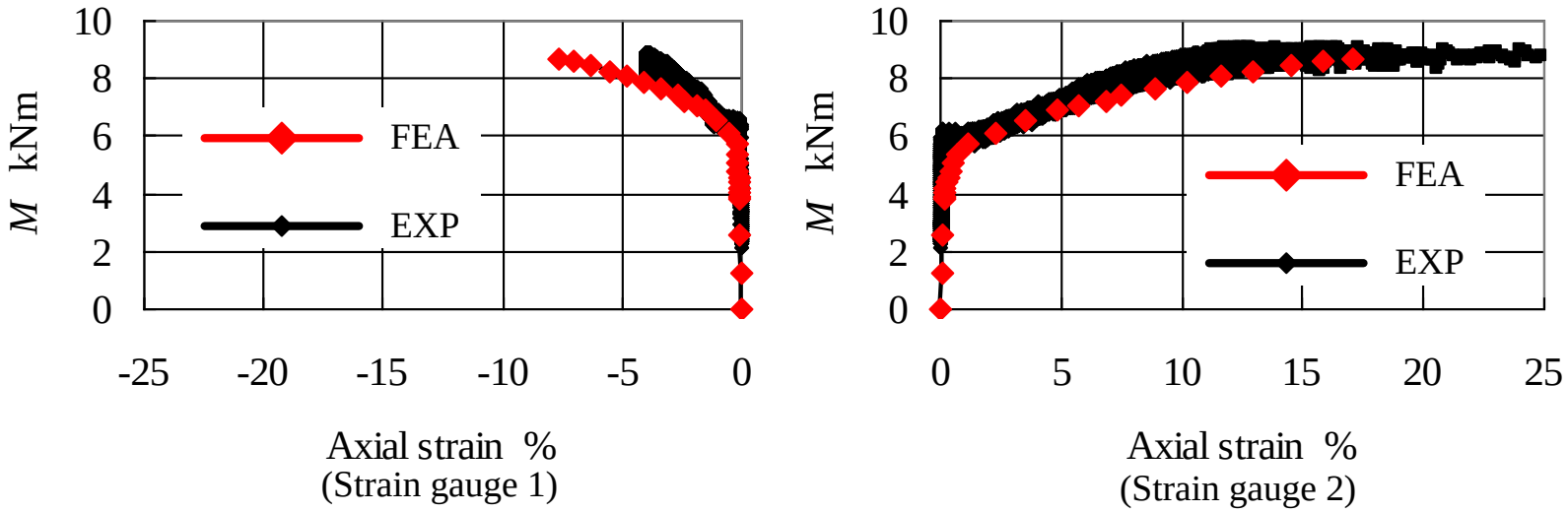

Fig. 11 Comparison of the FEA and experimental results: case of collapse (specimen no. 10-12)

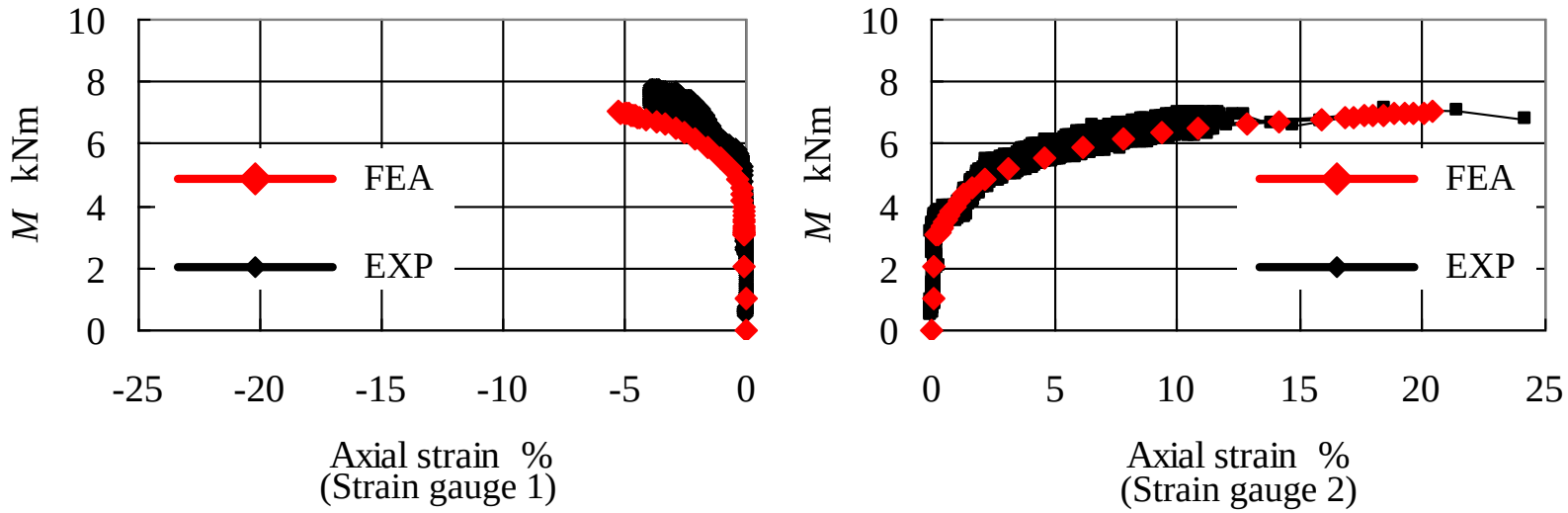

Fig. 12 Comparison of the FEA and experimental results: case of cracking (specimen no. 10-04)

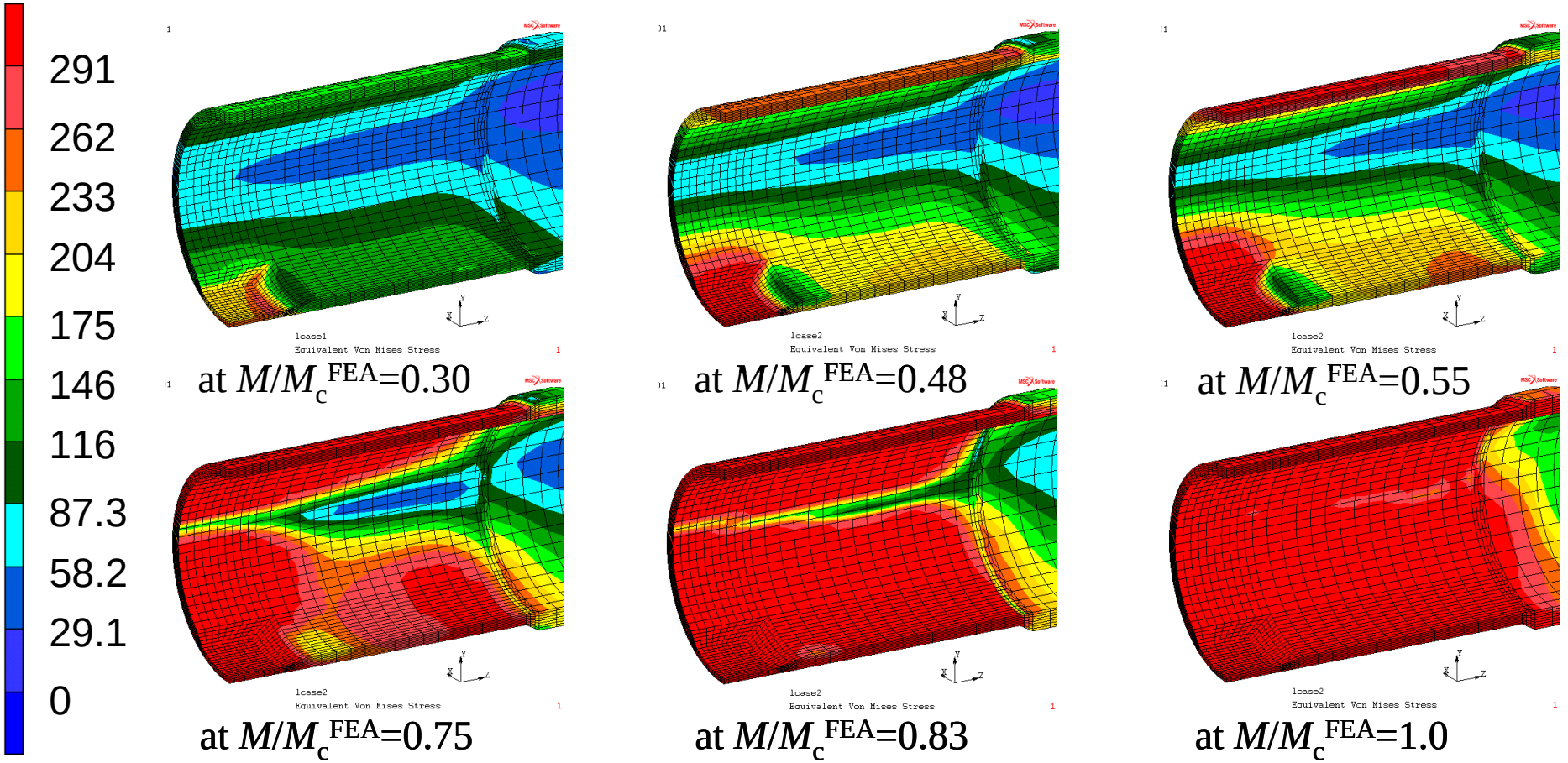

Fig. 13 The Mises stress distribution change for an increasing load
(case of collapse: $\delta_z/(\theta R_m)$=1.005 Spec.10-12)

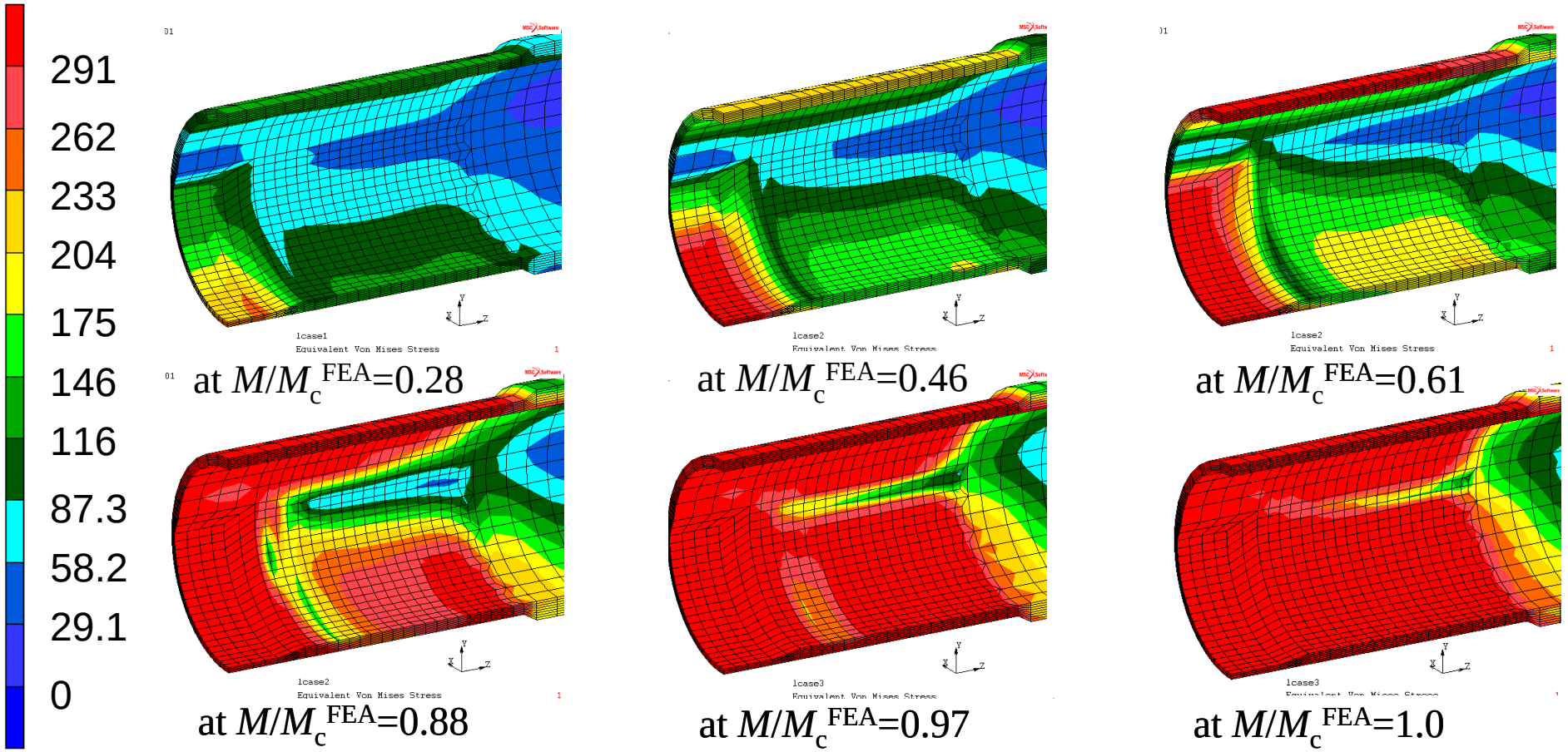

Fig. 14 The Mises stress distribution change for an increasing load
(case of cracking: $\delta_z/(\theta R_m)$=0.168 Spec.10-12)

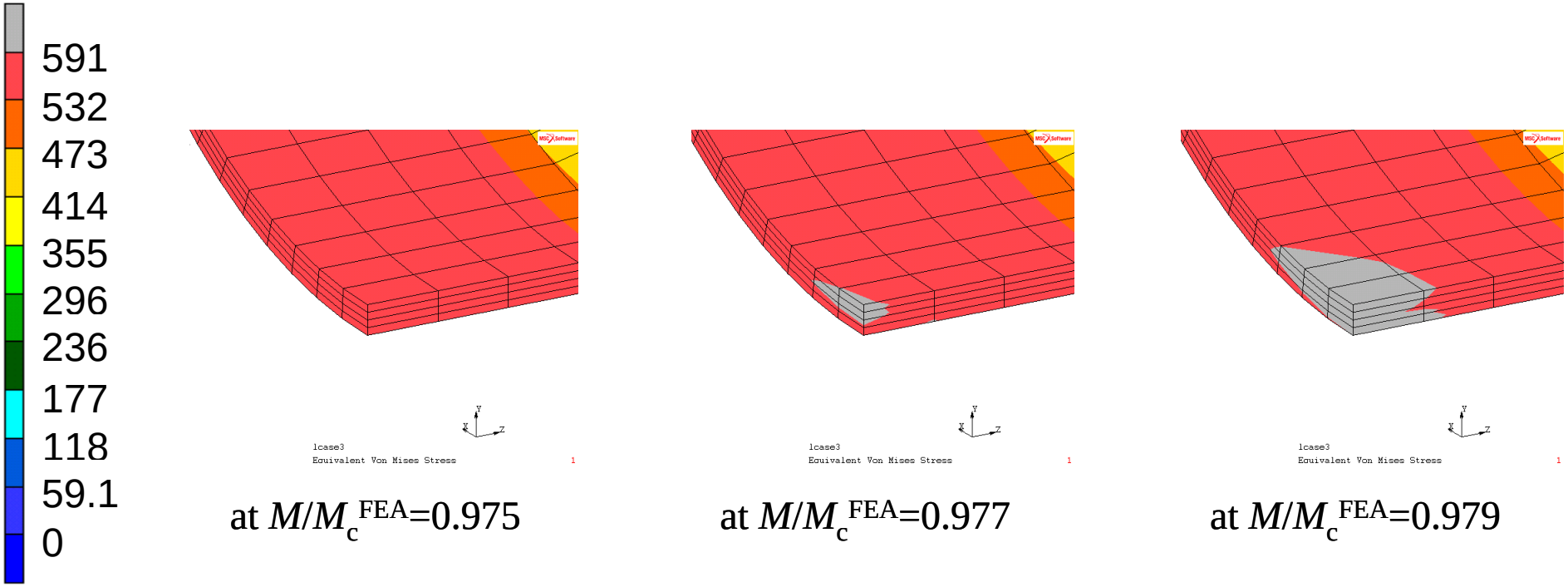

at M/M_c^{FEA}=0.975 at M/M_c^{FEA}=0.977 at M/M_c^{FEA}=0.979

Fig. 15 The Mises stress distribution at M_c^{FEA} (case of cracking: $\delta_z/(\theta R_m)$=0.168 Spec.10-04; 591 MPa is true tensile stress)

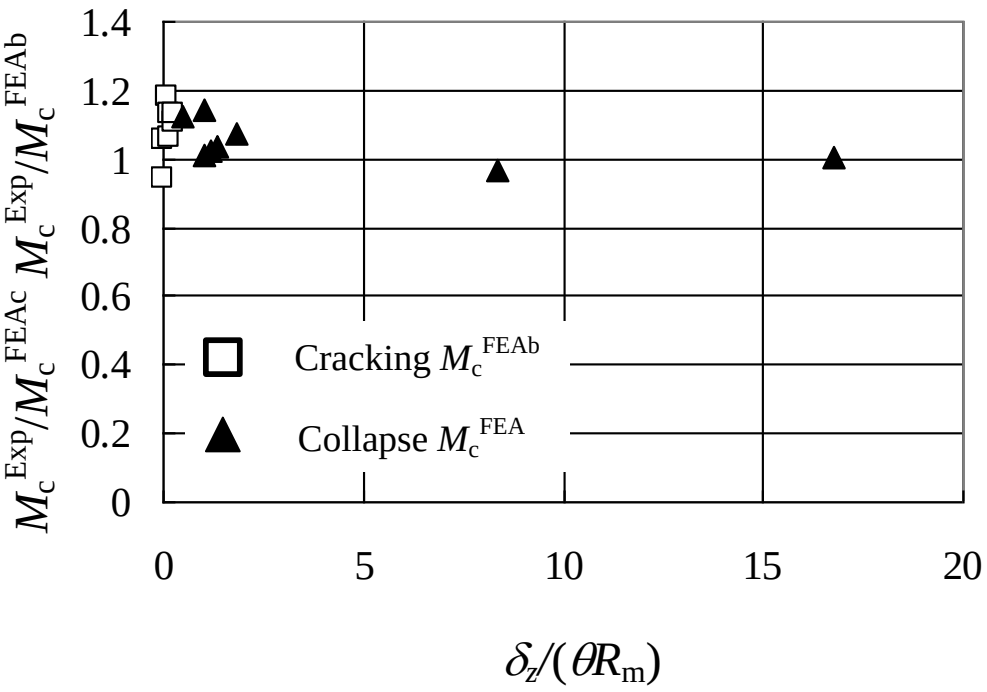

Fig. 16 Comparison of the limit bending load by DCC: M_c^{FEA}, M_c^{FEAb} and by experiment: M_c^{EXP}